Temporal temperature measurement on burning biomass pellets using phosphor thermometry and two-line atomic fluorescence

Weng, Wubin; Feuk, Henrik; Li, Shen; Richter, Mattias; Aldeń, Marcus; Li, Zhongshan

Published in:
Proceedings of the Combustion Institute

DOI:
10.1016/j.proci.2020.06.095

2021

Document Version:
Publisher's PDF, also known as Version of record

Available online at www.sciencedirect.com

ScienceDirect

Proceedings of the Combustion Institute 38 (2021) 3929–3938

Proceedings of the Combustion Institute

www.elsevier.com/locate/proci

Temporal temperature measurement on burning biomass pellets using phosphor thermometry and two-line atomic fluorescence

Wubin Weng, Henrik Feuk, Shen Li, Mattias Richter, Marcus Aldén, Zhongshan Li*

Division of Combustion Physics, Lund University, P. O. Box 118, SE-221 00 Lund, Sweden

Received 7 November 2019; accepted 28 June 2020
Available online 8 August 2020

Abstract

We report accurate *in-situ* optical measurements of surface temperature, volatile gas temperature, and polycyclic aromatic hydrocarbon (PAH) emission over the whole burning history of individual biomass pellets in various combustion atmospheres. Two biomass fuels, wood and straw, were prepared in cylindrical pellets of ∼300 mg. The pellets were burned in a well-controlled combustion atmosphere provided by a laminar flame burner with temperature ranging from 1390 K to 1840 K, and oxygen concentration from zero to 4.5%. The surface temperature of burning biomass pellets was accurately measured, for the first time, using phosphor thermometry, and the volatile gas temperature was measured using two-line atomic fluorescence thermometry. PAH emission was monitored using two-dimensional laser-induced fluorescence. During the devolatilization stage, a relatively low surface temperature, ∼700 K, was observed on the burning pellets. The volatile gas temperature was ∼1100 K and ∼1500 K 5 mm above the top of the pellets in a gas environment of ∼1800 K with 0.5% and 4.5% oxygen, respectively. PAH mainly released when the temperature of the pellet exceeded ∼600 K with the highest concentration close to the surface and being consumed downstream. The weight of the released PAH molecules shifted towards lighter with a reduction of gas environment temperature. The wood and straw pellets had almost the same surface and volatile gas temperature but different compositions in the released volatile gases. The temperature information provided in the present work aids in revealing the reactions in the burning biomass fuels regarding species release, such as various hydrocarbons, nitrogen compounds, and potassium species, and is valuable for further development of biomass thermal conversion models.

Keywords: Biomass combustion; Temperature; Phosphor thermometry; Two-line atomic fluorescence; PAH laser-induced fluorescence

* Corresponding author.
E-mail address: zhongshan.li@forbrf.lth.se (Z. Li).

https://doi.org/10.1016/j.proci.2020.06.095

1. Introduction

Biomass is a renewable and carbon-neutral energy source, which can provide heat and power through combustion, or biofuels through gasification. Understanding the thermal conversion processes of biomass is essential to achieve higher efficiency and lower emissions. However, the thermal conversion of solid biomass fuels is a complex phenomenon involving heterogeneous and homogeneous chemical reactions, heat and mass transfers, and phase transitions. Individually burning biomass pellets were investigated [1-3], to facilitate the fundamental understanding and to support the development of modeling [4,5]. Recently, advanced *in-situ* optical techniques have been developed to quantitatively measure the important species released from burning biomass pellets, such as potassium atoms [1] and HCN molecules [2]. However, accurate temperature is needed to correlate these valuable data into a deepened understanding of the reaction processes.

Thermocouples have been applied in temperature measurements either embedded in the center or attached on the surface of biomass samples [5-7]. However, perturbations are introduced through heat transfers and catalytic effects from the thermocouple wires. Pyrometer is a non-intrusive method and can be used to measure the surface temperature of burning biomass pellets [3,5]. However, during the devolatilization stage, the low-temperature surface only provides weak thermal radiation, which can barely be detected. The strong interference of the optical emissions from soot and hot burner walls can introduce significant uncertainties. To achieve an accurate surface measurement of biomass pellets over the whole burning history, in this work, for the first time, phosphor thermometry was employed, which can cover from cryogenic temperatures to above 1700 K [8]. Moreover, the temporal variation of the volatile gas temperature was recorded using two-line atomic fluorescence (TLAF) thermometry with indium atoms [9], which can provide spatially and temporally resolved measurements in particle-laden and sooty flames [10,11].

As dominant hydrocarbons in the volatile gases released from burning biomass, polycyclic aromatic hydrocarbons (PAHs) were measured using planar laser-induced fluorescence (PLIF), which were correlated to the obtained temperature information. The mass loss during the burning of the pellets was monitored in real-time using a weight scale. Well-defined combustion atmospheres were adopted. The temperature and oxygen concentration varied from 1390 K to 1840 K, and from zero to 4.5%, respectively, for a systematic investigation of the influence of the combustion atmosphere. For each case, the result with a standard deviation was obtained based on three repetitions. The experimental results, especially the accurate temperature information of the burning single biomass pellets newly obtained in the present work, can facilitate the fundamental understanding of the underlying thermal chemistry in the burning biomass fuels and the progress in modeling.

2. Experimental setup

2.1. Burner and flame conditions

A laminar flame burner, referred to as multi-jet burner [12], shown in Fig. 1a, was used to provide hot gas environments. In the jet chamber of the burner, the premixed CH_4/air/O_2 gas flow is distributed into 181 jet tubes. On the outlet of each tube, a premixed flame is stabilized. The co-flow gas, mainly N_2 and air, is introduced through the co-flow chamber and evenly distributed around each jet tube through a perforated plate. The mixture of the co-flow and the flue gas of the premixed jet flames generates the hot gas environments above the burner outlet, which has a size of 85 mm × 47 mm and is ∼29 mm above the outlets of the jet tubes. The hot flow has a mean speed of ∼1 m/s. A flow stabilizer is placed 35 mm above the burner outlet. The temperature of the flow stabilizer surface facing the hot flue gas was measured to be ∼800 K using a B type thermocouple (OMEGA). The flame conditions adopted in the present study are shown in Table 1. The gas temperatures in the table were measured using TLAF thermometry with indium atoms [9]. The biomass pellets were placed with their centers ∼5 mm above the burner outlet. The biomass pellets were cylindrical and weighed ∼300 mg each. Two types of biomass fuels, wood and straw, were investigated. The wood and straw pellets had sizes of around 6 mm × 10 mm and 8 mm × 5 mm (diameter × length), respectively, in similar volume and surface area. The properties of the biomass fuels are presented in Table S1 in the supplement. The biomass pellets were held by two ceramic rods of 1 mm in diameter, as shown in Fig. 1a. The rods were fixed on a weight scale (A&D company), and the mass loss of individually burning biomass pellets was monitored with a precision of 1 mg.

2.2. Phosphor thermometry

Phosphor thermometry, including the lifetime method and spectral method, has previously been applied to measure surface temperature on burning materials [13,14]. The lifetime method assesses the temperature by monitoring the phosphorescence lifetime, which is more sensitive at higher temperatures than the spectral method [15]. Two phosphors, Mg_4FGeO_6:Mn and YAG:Tb (Phosphor Technology), were used in this work with the

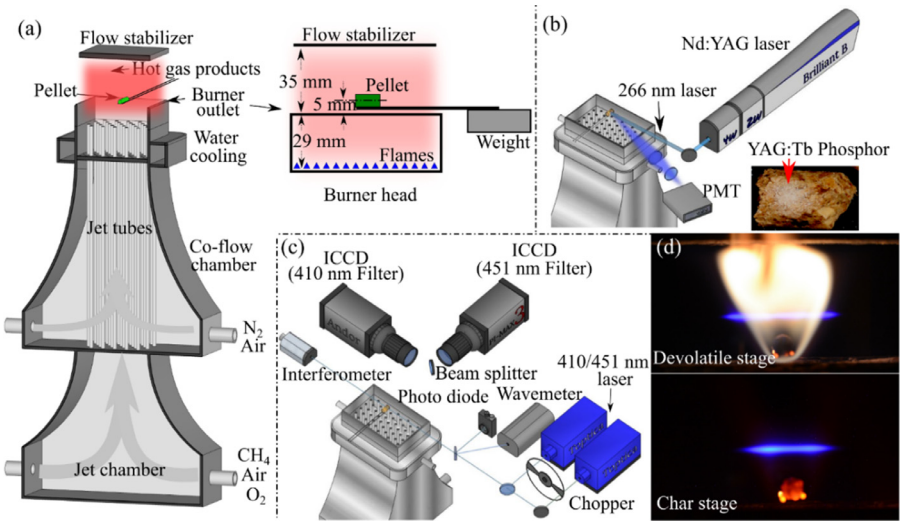

Fig. 1. Schematics of the multi-jet burner (a), the experimental setup of phosphor thermometry (b), TLAF thermometry (c), and the LIF images of atomic indium above the burning wood pellet at devolatilization and char stage (d).

Table 1
Summary of the flame conditions adopted in this experiment. The temperature was measured 5 mm above the burner outlet.

Flame Case	Gas flow rate (sl/min)					Fuel–air equivalence ratio ϕ	Gas product temperature (K)	O_2 in gas products (%)
	Jet-flow			Co-flow				
	CH_4	Air	O_2	N_2	Air			
T1O1	2.66	17.34	1.89	10.83	7.74	0.74	1750	4.5
T1O2	2.66	17.34	1.89	18.60	0.00	0.96	1790	0.5
T1O3	3.04	17.11	1.86	13.95	0.00	1.12	1840	0
T2O1	2.47	12.23	2.58	18.97	8.90	0.70	1550	4.5
T2O2	2.47	12.23	2.58	27.90	0.00	0.96	1530	0.5
T3O1	2.28	11.89	2.26	22.69	9.83	0.67	1390	4.5
T3O2	2.28	11.89	2.26	32.55	0.00	0.96	1400	0.5

lifetime method to measure surface temperatures of burning pellets from 300 K to 950 K, and from 850 K to 1300 K, respectively. The uncertainty, varied with phosphor sensitivity, was typically below 1% in temperature sensitive regions. The correlation between the decay time and the temperature was obtained using the calibration procedure reported by Nada et al. [16].

The phosphors were excited by a 266 nm beam from a 10 Hz Nd:YAG laser (Brilliant B) with 5 ns pulse duration. The pulse energy was 2.6 mJ for Mg_4FGeO_6:Mn and 3.0 mJ for YAG:Tb. The phosphorescence signal was detected using a photomultiplier tube (PMT, Hamamatsu H11526-20-NF). The PMT's gating functionality was used to temporally filter out short-lived components, including fluorescence and elastic laser scattering. Bandpass filters at 483 nm (FWHM = 31 nm) and 656 nm (FWHM = 10 nm) were used for the YAG:Tb and the Mg_4FGeO_6:Mn phosphor, respectively, to isolate the phosphorescence emission band with the appropriate temperature sensitivity and signal strength. The PMT signal was connected to an oscilloscope using a 50 Ω input resistance.

The phosphor powder was mixed with HPC binder (ZYP Coatings Inc.) and applied as approximately 4 mm diameter spots to the surface of the pellets. When conducting phosphor thermometry, it is desirable to keep the phosphor coating thin to minimize potential temperature gradients across the sensor material. The mean thickness of the layer was estimated to be around 2 μm and should, therefore, give negligible temperature gradients. The influence of the phosphor on the char oxidation was also observed to be negligible, as at this stage, only dispersed phosphor particles remained on the pellet surface. During the combustion, the phosphorescence signal could decrease due to loss of phosphor particle or absorption and scattering from volatile gas, but it has no direct influence on the decay time and the temperature mea-

surement. Only one phosphor was applied on a pellet at a time to reduce experimental complexity. For each flame condition, both phosphors were used on three pellets using the setup shown in Fig. 1b.

2.3. Two-line atomic fluorescence

Two-line atomic fluorescence thermometry was adopted to measure the gas temperature above the burning biomass pellet, as shown in Fig. 1c. Two continuous-wave diode lasers (Toptica, DL100pro and DL100) produced ~5 mW laser beams at 410 nm and 451 nm. The beams were overlapped using a dichroic mirror and passed 5 mm above the top of the biomass pellets. Into the volatile plume, indium atoms were continuously released from the ceramic rods beneath the biomass pellet as the tips of the rods had been dipped into an indium chloride ($InCl_3$) water solution. The indium atoms were excited to a common upper level from two different lower levels by the 410 and 451 nm laser with transitions $5^2P_{1/2} \rightarrow 6^2S_{1/2}$ and $5^2P_{3/2} \rightarrow 6^2S_{1/2}$, respectively. Typical photos with the LIF signal above the biomass pellet at volatile and char burning stages are presented in Fig. 1d. In order to eliminate the influence of elastic scattering, LIF signals from non-resonant transitions were collected to derive the temperature. Two ICCD cameras (Andor iStar, and Princeton PI-MAX II, 1024 × 1024 pixels) with filters centered at 410 nm and 450 nm (FWHM = 10 nm) were used. The laser power and wavelength were monitored by a photodiode (PDA100A2, Thorlabs) and a wavemeter (HighFinesse UV6-200). The two lasers switched with a time gap of 14 ms and at 7 Hz using a beam chopper. The cameras were synchronized with the lasers and had an exposure time of 1 ms. Since the time gap was quite short, there was almost no influence from the slow fluctuation of the volatile gas plume in the measurement. The two cameras were calibrated to compensate for differences in detection efficiency. The temperature derivation was reported by Borggren et al. [9], and the uncertainty was around ±3%.

2.4. Planar laser-induced fluorescence of PAH

The distribution of the PAH released from the burning biomass pellet during the devolatilization stage was visualized using PLIF. The third and fourth harmonic of a Nd:YAG laser (Brilliant B) provided the 355 nm and 266 nm laser pulse, respectively, which were used as the excitation source separately. The laser beam was formed into a laser sheet of ~1 mm thickness above the burning biomass pellet in the vertical plane. The fluorescence at 410 nm and 515 nm was captured by an ICCD camera (Andor iStar) simultaneously through a stereoscope lens having 410 nm and 515 nm band-pass filters (FWHM = 10 nm) in each channel. The signal acquisition frequency was 3 Hz. The laser fluence for 266 nm and 355 nm laser beam at the probe location was ~3.6 mJ/cm^2 and ~9 mJ/cm^2, respectively. The laser-induced incandescence of soot was negligible due to low laser fluence, and small gate-width of the camera of 20 ns, without delay.

3. Results and discussion

The surface temperature of individually burning biomass pellets in different hot gas environments over the burning time is shown in Fig. 2. The burning process was separated into two stages, i.e. devolatilization and char conversion indicated by the vertical dash lines in Fig. 2. The burning phase was shifted from devolatilization to char conversion as the mass loss rate of the burning biomass pellets (cf. Fig. 5) reduced to below 1 mg/s. The measurement position was located at the side of the pellet, as shown in Fig. 1b. Immediately after being introduced into the hot gas flow, the pellet was heated up, and the surface temperature increased from room temperature to ~600 K in the first 10 s (cf. Fig. 2). When the temperature exceeded 600 K, decomposition [17] occurred in the wood pellet, and volatile gases were released. Since this is an endothermic process, only a mild increase in temperature was observed until the devolatilization stage ended at ~60–70 s. A decline of ~150 K on the surface temperature was observed, when the gas environment temperature reduced by 400 K through switching from case T1O2 to T3O2, as shown in Fig. 2a and 2c. Higher surface temperature was observed under the conditions with 4.5% oxygen compared to the conditions with 0.5% oxygen (cf. Fig. 2b), since under the former conditions, volatile gases burnt above the pellets (cf. Fig. 1d), providing additional heat to the pellets. In cases of T1O2 to T3O2, the hot surrounding gas contained almost zero oxygen to oxidize the volatile gases. Comparing wood and straw pellets, similar surface temperatures were observed (cf. Fig. 2a and 2d). After the devolatilization stage, the surface temperature quickly increased, and char burning started.

During the whole char burning stage, the surface temperature almost remained constant and was ~500 K lower than the hot surrounding gas, as shown in Fig. 2b and 2c. It should be noted that for the cases T1O1 and T1O2, the surface temperature of the burning chars is absent (cf. Fig. 2a) since the measured decay time was shorter than the calibration data, but the surface temperature could be estimated to be approximately 1400 K by extrapolating the present data supported by previous calibrations on the phosphor [18]. The surface temperature was lower than the surrounding gas temperature, which indicates that the burning char had significant heat losses through thermal radiation and heat conduction through the holders. The char burning in the cases with 4.5% oxygen had

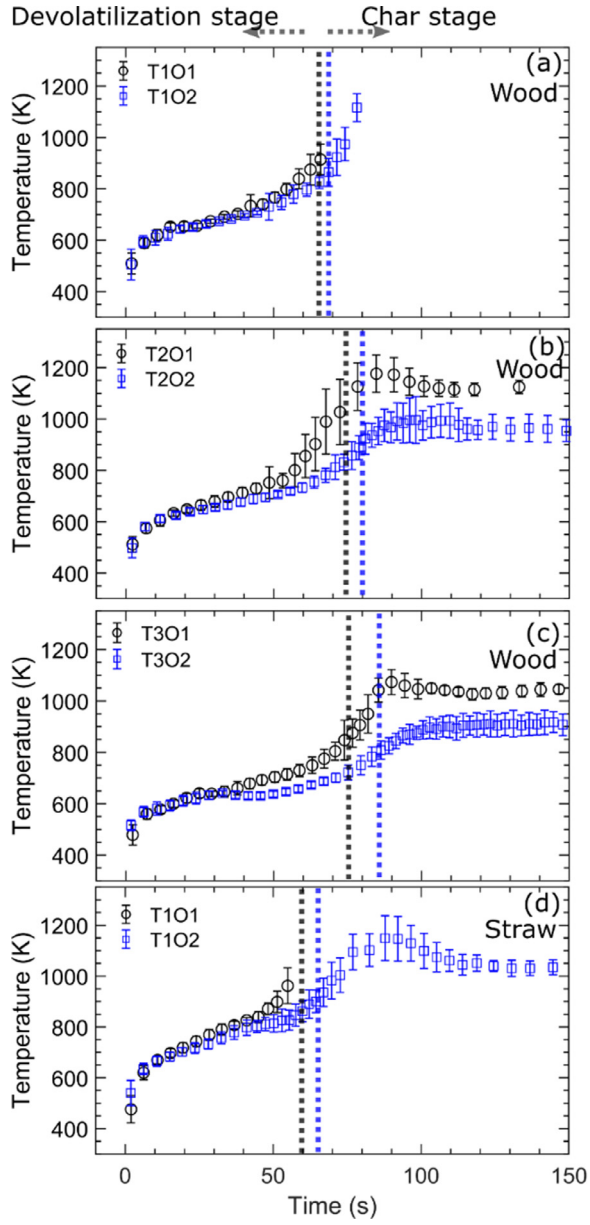

Fig. 2. Surface temperatures of individually burning biomass pellets in different hot gas environments over the burning time. Vertical dash lines separate the devolatilization stage and the char stage.

a surface temperature ~100 K higher than with 0.5% oxygen (cf. Fig. 2b and 2c), because the 4.5% oxygen case was dominated by the exothermic char oxidation reactions, while the 0.5% oxygen case was dominated by the endothermic steam gasification reaction $C + H_2O \rightarrow CO + H_2$, and the Boudouard reaction $C + CO_2 \rightarrow 2CO$ [19]. Straw pellets had lower surface temperature than wood pellets during the char burning stage (cf. Fig. 2a and 2d), which might be caused by the higher ash content in straw.

At 5 mm above the pellet, the temperature of the volatile gases was measured using TLAF thermometry. The horizontal distribution of the temperature along the laser beam (see LIF images in Fig. 1d) is presented in Fig. 3. In the devolatilization stage at 10, 40, and 65 s, the volatile gas temperature, ~1200 K at the center, was significantly lower

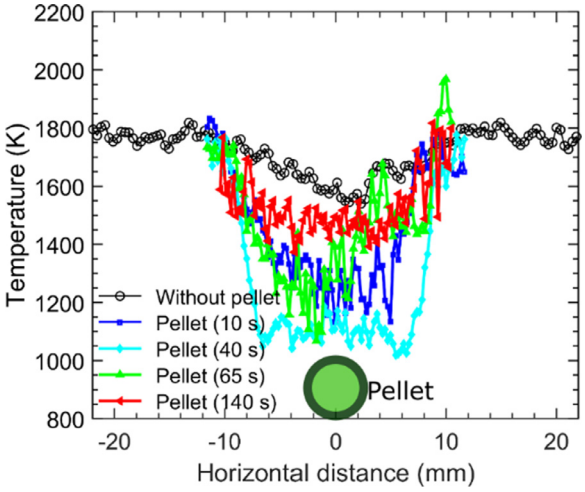

Fig. 3. Temperature distribution of the gas 5 mm above an individually burning wood pellet in the hot flue gas of flame T1O2 ($T = 1790$ K, ϕ=0.96) at the devolatilization stage (10, 40, and 65 s) and the char stage (140 s) measured with TLAF.

than the surrounding gas temperature, but ~400 K higher than the surface temperature of the pellets presented in Fig. 2. The lowest gas temperature in the center of volatile gas was observed at 40 s. At this moment, the rate of the volatile release was the greatest according to the mass loss rate curve in Fig. 5. The highest rate of volatile release led to the least amount of hot flue gas being entrained into the center of the low-temperature volatile gas. From the temperature distribution, the size of the volatile gas plume above the pellet spreads over 10 mm. During char burning, e.g. at 140 s, the temperature above the pellet increased to ~1500 K, while still lower than the surrounding gas temperature. The temperature decreased ~200 K with only the introduction of the ceramic holder into the hot gas flow as shown in Fig. 3.

The gas temperatures at the center of the volatile gas plume 5 mm above the top of the pellets in different hot gas environments as a function of the residence time are shown in Fig. 4. For the case T1O2 with 0.5% oxygen, the volatile gas temperature kept ~1200 K. As the volatile gas release finished at ~70 s, the temperature above the pellets increased to ~1400 K. For the case T1O1 with 4.5% oxygen, volatile gas flames were stabilized above the pellets with a temperature of ~1500 K. The volatile gas temperatures decreased when the surrounding gas temperature reduced (cf. Fig. 4a-4c), similar to the surface temperature as shown in Fig. 2a-2c. The wood and straw pellets almost had the same volatile gas temperature (cf. Fig. 4a and 4d).

Since around 80% (dry basis) of the mass of the biomass fuels was in the form of volatile (see Table S1 in the supplemental material), the mass loss mainly occurred in the devolatilization stage. As shown in the inset of Fig. 5a, the initial mass of the pellet was ~300 mg, and after the devolatilization, only ~45 mg char was left. The mass loss started with the increase of the surface temperature (cf. Fig. 2) as the pellets were introduced into the hot gas environment, and the mass-loss rate increased and reached its maximum of ~6 mg/s at ~40 s. The hot gas environment temperature and oxygen concentration could slightly affect the mass loss process (cf. Fig. 5a-5c). With a higher temperature and oxygen concentration, the mass drop started earlier and the devolatilization time decreased. The straw and wood pellets had similar mass loss processes (cf. Fig. 5a and 5d).

In order to the correlate the volatile gas release with the measured surface and volatile gas temperature, the distribution of PAH in the volatile gas and the release history in different hot gas environments was obtained and is shown in Fig. 6. The fluorescence signals at 410 nm and 515 nm indicate relatively light and heavy PAH molecules, respectively [20]. Typical images of the PAH LIF signal at 410 nm are presented as the insets in Fig. 6a, where the pellet had the residence time of 40 s in the hot gas environments. The PAH mainly existed in the region close to the surface of the pellets and was consumed quickly downstream. Much less PAH LIF signal was observed in the gas environment with 4.5% oxygen than that with 0.5% oxygen. With more oxygen, the volatile gas temperature increased, from ~1200 K to ~1500 K (cf. Fig. 4a). Thus, the fluorescence quantum yield could be halved [21]; more PAH was transformed into soot [22] and oxidized by the oxygen diffused from the surrounding gas.

The total PAH LIF signal as a function of the residence time in different hot gas environments with standard deviation from three measurements

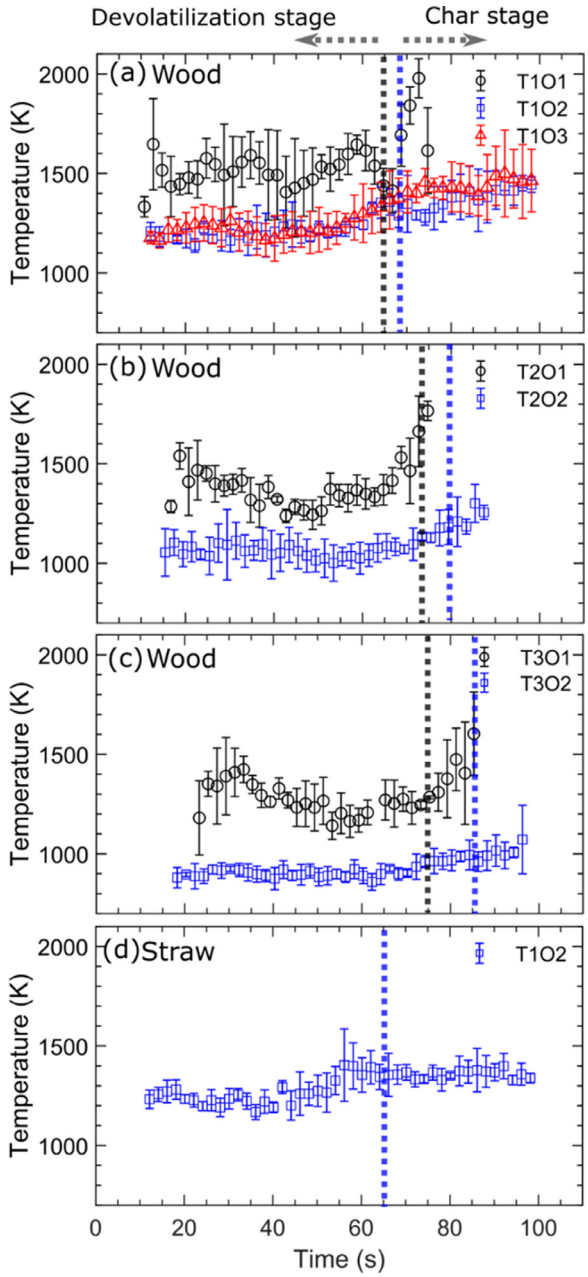

Fig. 4. Temperatures of the volatile gas 5 mm above individually burning biomass pellets in different hot gas environments as a function of the residence time. Vertical dash lines separate the devolatilization stage and the char stage.

was used to present the PAH release history, as shown in Fig. 6. The signal trends were close to the mass loss rate shown in Fig. 5 except in the first ~10 s, where no PAH release was observed. Hence, mainly drying and dehydration reactions occurred in this period at the temperature below ~600 K. After ~10 s, the PAH started to appear and the surface temperature exceeded ~600 K (cf. Fig. 2). The LIF signal had its maximum value at around 40 s and disappeared at the end of the devolatilization stage. For cases with 4.5% oxygen (cf. Fig. 6a, 6b, 6d and 6e), the signal trend was almost independent of temperature, except some increase due to higher fluorescence quantum yield at a lower

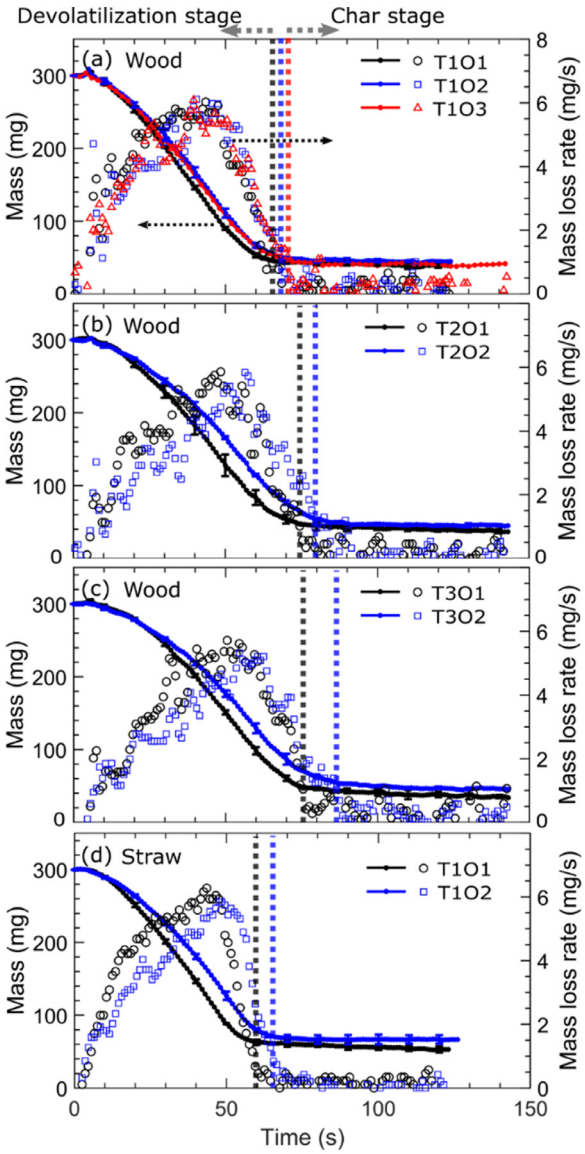

Fig. 5. Mass and mass-loss rates of individually burning biomass pellets in different hot gas environments as a function of the residence time from the devolatilization stage to the char stage. Vertical dash lines separate the devolatilization stage and the char stage.

temperature. However, in cases with 0.5% oxygen (cf. Fig. 6a, 6b, 6d and 6e), less LIF signal was obtained when the surrounding gas temperature became lower, especially at 515 nm. According to the mass loss measurements (cf. Fig. 5), a similar amount of volatile gases was released at all gas environment temperatures. Since more significant reduction occurred for the 515 nm fluorescence, the released PAH appears to shift towards lighter molecules with a reduction of ~100 K and ~200 K in surface and volatile gas temperature due to lower gas environment temperatures [23]. The straw pellets have a lower PAH signal than that for the wood pellets (cf. Fig. 6a, 6c, 6d and 6f), even though they had similar surface temperature, volatile gas temperature, and mass loss rate, as shown in Fig. 2, 4 and 5. It indicates that different volatile gases were generated in the pyrolysis of wood and straw, which might be due to the significant difference in ash content and composition shown in Table S1, especially potassium and sodium with its catalytic effect [24].

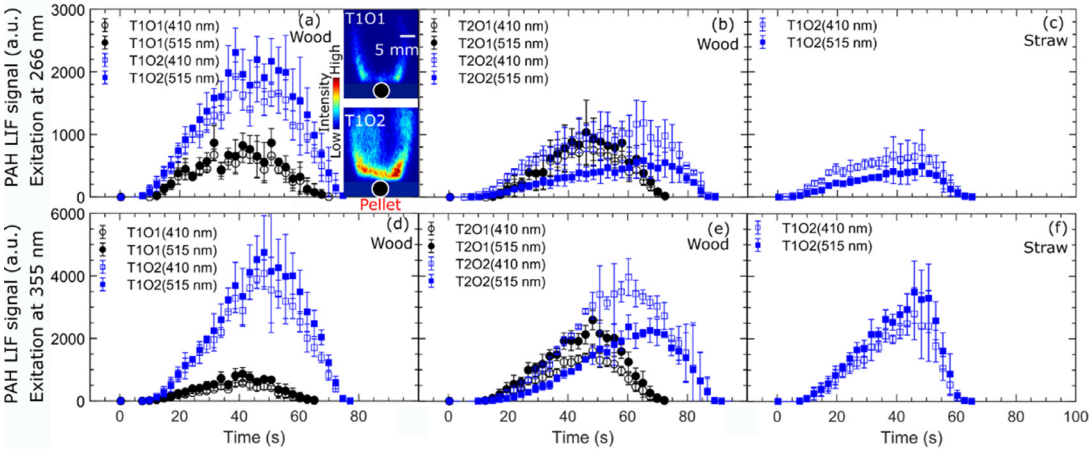

Fig. 6. PAH LIF signal in the volatile gases above individually burning biomass pellets in different hot gas environments as a function of residence time. Excitation was performed at 266 nm (a–c) and 355 nm (d–f). Insets in (a): LIF images at 410 nm of burning biomass pellets at the residence time of 40 s.

4. Conclusions

Single biomass pellets were burned in well-defined hot gas environments provided by a laminar flame burner, with varied temperatures from 1390 K to 1840 K and oxygen concentrations from zero to 4.5%. Temporally resolved surface temperature and volatile gas temperature of individually burning biomass pellets were recorded using phosphor thermometry and two-line atomic fluorescence thermometry, respectively. The spatial distribution of PAH molecules in the volatile gas was recorded using two-dimensional LIF. The mass loss of the burning pellet was monitored by a weight scale.

After a drying of ~10 s with a quick increase of the surface temperature to ~600 K, PAH started to release, with a constant temperature around 700 K until the end of the devolatilization stage. The PAH in the volatile gases mainly distributed close to the surface of the pellets before being consumed downstream. During the char conversion, the surface temperature significantly increased but was still ~500 K lower than the hot gas environment. Comparing with the cases with 0.5% oxygen in the hot gas environments, the cases with 4.5% oxygen introduced higher volatile gas temperature and surface temperature due to the volatile gas burning above the pellets. The gas environments with higher temperature also led to higher surface temperature and volatile gas temperature. As the surface temperature and volatile gas temperature decreased with the gas environment temperature, the released PAH was detected to shift towards lighter molecules. The burning wood and straw pellets had almost no difference in surface temperature, volatile gas temperature, and mass loss rate, but the released volatile gas composition differed.

In a future study, with the measurement of gas composition such as HCN and NH_3 important for nitrogen reaction mechanism using IR-DFWM, different alkali species using 2D-LIPF [25] and TD-LAS [1], and different PAH molecules using LIF, the accurate temperature information obtained in the present work enables quantitative analysis of the underlying thermal chemistry in the burning biomass fuels and progress in modelling.

Declaration of Competing Interest

None.

Acknowledgments

This work was supported by the Swedish Research Council (VR), the European Research Council, the Knut & Alice Wallenberg Foundation, and the Swedish Energy Agency (STEM) through the KC-CECOST project. We thank Peter Glarborg and Hao Wu from the Technical University of Denmark for providing the well characterized biomass material and fruitful discussions.

Supplementary materials

Supplementary material associated with this article can be found, in the online version, at doi:10.1016/j.proci.2020.06.095.

References

[1] W. Weng, Q. Gao, Z. Wang, R. Whiddon, Y. He, Z. Li, M. Aldén, K. Cen, *Energy Fuels* 31 (2017) 2831–2837.

[2] D. Hot, R.L. Pedersen, W. Weng, Y. Zhang, M. Aldén, Z. Li, *Proc. Combust. Inst.* 37 (2019) 1337–1344.
[3] Y. Liu, Z. Wang, J. Xia, L. Vervisch, K. Wan, Y. He, R. Whiddon, H. Bahai, K. Cen, *Proc. Combust. Inst.* 37 (2019) 2681–2688.
[4] H. Fatehi, X.S. Bai, *Combust. Sci. Technol.* 186 (2014) 574–593.
[5] H. Lu, W. Robert, G. Peirce, B. Ripa, L.L. Baxter, *Energy Fuels* 22 (2008) 2826–2839.
[6] J.T. Kuo, C.-.L. Hsi, *Combust. Flame* 142 (2005) 401–412.
[7] W.C. Park, A. Atreya, H.R. Baum, *Combust. Flame* 157 (2010) 481–494.
[8] S.W. Allison, G.T. Gillies, *Rev. Sci. Instrum.* 68 (1997) 2615–2650.
[9] J. Borggren, W. Weng, A. Hosseinnia, P.-.E. Bengtsson, M. Aldén, Z. Li, *Appl. Phys. B* 123 (2017) 278.
[10] J. Borggren, W. Weng, M. Aldén, Z. Li, *Appl. Spectrosc.* 72 (2017) 964–970.
[11] D. Gu, Z. Sun, B.B. Dally, P.R. Medwell, Z.T. Alwahabi, G.J. Nathan, *Combust. Flame* 179 (2017) 33–50.
[12] W. Weng, J. Borggren, B. Li, M. Aldén, Z. Li, *Rev. Sci. Instrum.* 88 (2017) 045104.
[13] A. Omrane, F. Ossler, M. Aldén, *Proc. Combust. Inst.* 29 (2002) 2653–2659.
[14] A. Omrane, F. Ossler, M. Aldén, U. Gtoransson, G. Holmstedt, *Fire Saf. Sci.* 7 (2003) 141–152.
[15] N. Fuhrmann, J. Brübach, A. Dreizler, *Proc. Combust. Inst.* 34 (2013) 3611–3618.
[16] F.A. Nada, C. Knappe, X. Xu, M. Richter, M. Aldén, *Meas. Sci. Technol.* 25 (2014) 025201.
[17] W.-.J. Liu, W.-.W. Li, H. Jiang, H.-.Q. Yu, *Chem. Rev.* 117 (2017) 6367–6398.
[18] M. Aldén, A. Omrane, M. Richter, G. Särner, *Prog. Energy Combust. Sci.* 37 (2011) 422–461.
[19] T. Li, Y. Niu, L. Wang, C. Shaddix, T. Løvås, *Appl. Energy* 227 (2018) 100–107.
[20] A. Ciajolo, A. D'Anna, R. Barbella, *Combust. Sci. Technol.* 100 (1994) 271–281.
[21] Y. Zhang, L. Wang, P. Liu, Y. Li, R. Zhan, Z. Huang, H. Lin, *Appl. Phys. B* 125 (2018) 6.
[22] G. Blanquart, H. Pitsch, *Combust. Flame* 156 (2009) 1614–1626.
[23] C. Brackmann, M. Aldén, P.-.E. Bengtsson, K.O. Davidsson, J.B.C. Pettersson, *Appl. Spectrosc.* 57 (2003) 216–222.
[24] H. Thunman, M. Seemann, T. Berdugo Vilches, J. Maric, D. Pallares, H. Ström, G. Berndes, P. Knutsson, A. Larsson, C. Breitholtz, O. Santos, *Energy Sci. Eng.* 6 (2018) 6–34.
[25] W. Weng, Y. Zhang, H. Wu, P. Glarborg, Z. Li, *Fuel* 271 (2020) 117643.